

Design and tests of the hard X-ray polarimeter X-Calibur

M. Beilicke^a, M.G. Baring^b, S. Barthelmy^c, W.R. Binns^a, J. Buckley^a, R. Cowsik^a,
 P. Dowkontt^a, A. Garson^a, Q. Guo^a, Y. Haba^d, M.H. Israel^a, H. Kunieda^d, K. Lee^a,
 H. Matsumoto^d, T. Miyazawa^d, T. Okajima^c, J. Schnittman^c, K. Tamura^d, J. Tueller^c, and
 H. Krawczynski^a

^aDepartment of Physics and McDonnell Center for the Space Sciences, Washington University,
 St. Louis, MO, USA; ^bRice University, TX, USA; ^cGoddard Space Flight Center, MD, USA;
^dNagoya University, Japan;

ABSTRACT

X-ray polarimetry promises to give qualitatively new information about high-energy astrophysical sources, such as binary black hole systems, micro-quasars, active galactic nuclei, and gamma-ray bursts. We designed, built and tested a hard X-ray polarimeter *X-Calibur* to be used in the focal plane of the InFOC μ S grazing incidence hard X-ray telescope. *X-Calibur* combines a low-Z Compton scatterer with a CZT detector assembly to measure the polarization of 10 – 80 keV X-rays making use of the fact that polarized photons Compton scatter preferentially perpendicular to the electric field orientation. *X-Calibur* achieves a high detection efficiency of order unity.

Keywords: X-rays, polarization, black hole, InFOCuS, X-Calibur

1. INTRODUCTION

Motivation. Spectral and morphological studies in the X-ray energy band (and above) have become established tools to study the non-thermal emission processes of various astrophysical sources. However, many of the regions of interest (black hole vicinities, jet formation zones, etc.) are too small to be spatially resolved with current and future instruments. Spectropolarimetric X-ray observations are capable of providing additional information – namely the fraction and orientation of linearly polarized photons – and would help to constrain different emission models¹ of sources with compact emission regions and high X-ray fluxes such as mass-accreting black holes (BHs) and neutron stars. So far, only a few missions have successfully measured polarization in the soft (OSO-8²) and hard (Integral³) X-ray energy regime. The Crab nebula is the only source for which the polarization of the X-ray emission has been established with a high level of confidence.^{2,3} The source exhibits a polarization fraction of 20% at energies of 2.6 – 5.2 keV (direction angle of 30 deg with respect to the X-ray jet)² and $46\% \pm 10\%$ above 100 keV (direction aligned with the X-ray jet observed in the nebula). Integral observations of the X-ray binary Cygnus X-1 indicate a high fraction of polarization in the hard X-ray/gamma-ray bands.⁴ Model predictions of polarization fraction for various source types lie slightly below the sensitivity of the past OSO-8 mission, making future, more sensitive polarimeter missions particularly interesting.

Future missions. As polarimetry was not the main objective of the Integral mission, the results are plagued by large systematic uncertainties, and there are currently no other missions in orbit that are capable of making sensitive X-ray polarimetric observations. This will change by the launch of the satellite-borne *Gravity and Extreme Magnetism SMEX* (GEMS) mission⁵ scheduled for 2014. GEMS will use two Wolter-type X-ray mirrors to focus 2 – 10 keV photons onto photo-effect polarimeters. For higher energies $E > 10$ keV X-ray polarimeter designs usually make use of the Compton effect: photons scatter preferentially perpendicular to the orientation of the electric field vector – the azimuthal distribution of scattered events will therefore show a sinusoidal modulation with 180 deg periodicity and a maximum at ± 90 deg to the preferred electric field direction of a polarized X-ray signal. The *Soft Gamma-Ray Imager* on *ASTRO-H*⁶ (launch scheduled for 2013) will have capabilities of measuring polarization, but the results may be plagued by similar systematic uncertainties as with the Integral

Further author information: (Send correspondence to M. Beilicke): beilicke@physics.wustl.edu

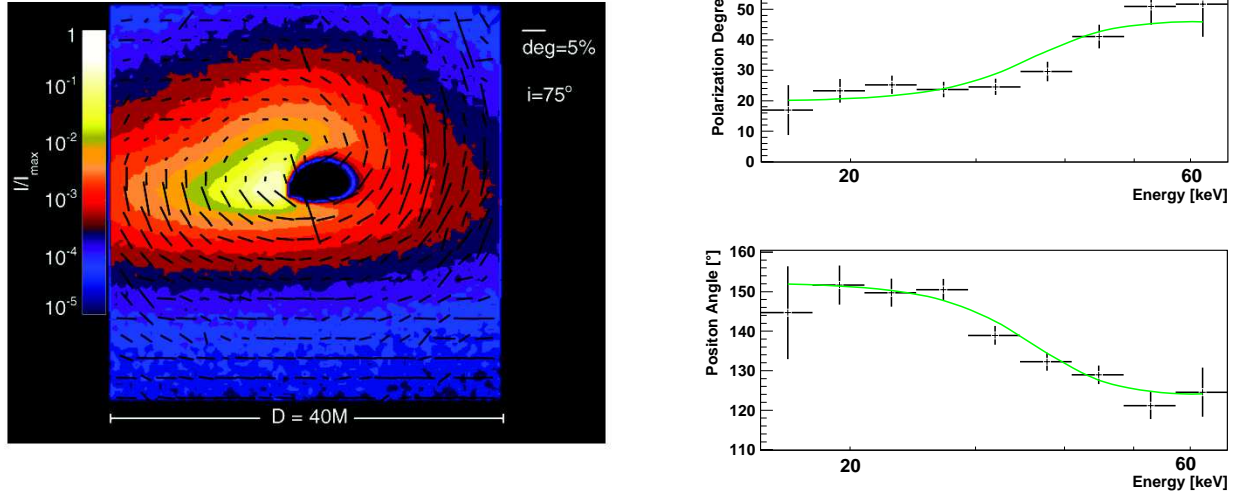


Figure 1. **Left:** Ray-traced image of direct radiation from a thermal disk around a black hole including returning radiation (observer located at an inclination angle of 75 deg, gas on the left side of the disk moving toward the observer causing the characteristic increase in intensity due to relativistic beaming). The observed intensity is color-coded on a logarithmic scale and the energy-integrated polarization vectors are projected onto the image plane with lengths proportional to the fraction of polarization. The image has been adopted from Schnittman et al. (2009).⁷ **Right:** Simulated X-Calibur observations of the Crab (5.6 h) as discussed in Sec. 3. The data points show the reconstructed fraction of polarization (top) and polarization angle (bottom) for the assumed model (solid lines).

results. The hard X-ray polarimeter *X-Calibur* discussed in this paper has the potential to cover the energy range above 10 keV. Furthermore, X-Calibur combines a high detection efficiency with a low level of background and has well-controlled systematic errors. These features make it a particularly useful instrument for astronomical X-ray polarimetry.

Scientific potential. Polarization measurements are of general interest as tests of non-thermal emission processes in the Universe. Synchrotron emission, for example, will result in linearly polarized photons with their electric fields oriented perpendicular to the magnetic field lines (projected) and the observed polarization map in the X-rays can therefore be used to trace the magnetic field structure of the source. An electron population with a spectral energy distribution of $dN/dE \propto E^{-p}$ emitting in a uniform magnetic field will lead to an observable fraction of polarization⁸ of $f_{\text{sync}} = (p+1)/(p+7/3)$ with $(p+3) = (\alpha+1)/(\alpha+5/3)$, where α is the index of the X-ray power spectrum. An observed polarization fraction close to this limit can therefore be interpreted as an indication of a highly ordered magnetic field since non-uniformities in the magnetic field will reduce the fraction of polarization. The polarized synchrotron photons can be inverse-Compton (IC) scattered by relativistic electrons – weakening the fraction of polarization (but not erasing it) and imprinting a scattering angle dependence⁹ to the observed fraction of polarization. Such IC signals usually (but not always) appear in hard gamma-rays, where polarimetry is difficult, due to multiple scattering in pair production detectors. Another important mechanism for polarizing photons is Thomson scattering which creates a polarization perpendicular to the scattering plane. Curvature radiation is polarized, as well. The scientific potentials of spectro-polarimetric hard X-ray observations are listed below:

- *Binary black hole systems.* Particle scattering within a Newtonian accretion disk will lead to the emission of polarized X-rays. Relativistic aberration and beaming, gravitational lensing, and gravitomagnetic frame-dragging will result in an energy-dependent fraction of polarization¹⁰ since photons with higher energies originate closer to the BH than the lower-energy photons. Schnittman and Krolik^{7, 11} calculate the expected

polarization signature including the effects of deflection of photons emitted in the disk by the strong gravitational forces in the regions surrounding the black hole and of the re-scattering of these photons by the accretion disk. The resultant effect is a swing in the polarization direction from being horizontal at low energies to being vertical at high energies, i.e., parallel to the spin axis of the black hole. Spectropolarimetric observations can therefore be used to constrain the mass and spin of the BH,⁷ as well as the inclination of the inner accretion disk and the shape of the corona¹¹ (Fig. 1, left).

- *Pulsars and pulsar wind nebulae.* High-energy particles in pulsar magnetospheres are expected to emit synchrotron and/or curvature radiation which are difficult to distinguish from one another, solely based on the observed photon energy spectrum. However, since the orbital planes for accelerating charges that govern these two radiation processes are orthogonal to each other, their polarized emission will exhibit different behavior in position angle and polarization fraction as functions of energy and the phase of the pulsar.³ In magnetars, the highly-magnetized cousins of pulsars, polarization-dependent resonant Compton up-scattering is a leading candidate for generating the observed hard X-ray tails (e.g. Baring & Harding 2007¹²). In both these classes of neutron stars, phase-dependent spectropolarimetry can probe the emission mechanism, and provide insights into the magnetospheric locale of the emission region. Furthermore, spectropolarimetric observations can be used to constrain the magnetic field and particle populations in pulsar wind nebulae such as the Crab, the leading driver for this field of X-ray polarimetry. These objects potentially show a higher polarization fraction at hard X-rays as compared to soft X-rays, reflecting the contrast between jet and more diffuse nebular contributions.
- *Relativistic jets in active galactic nuclei.* Relativistic electrons in jets of active galactic nuclei (AGN) emit polarized synchrotron radiation at radio/optical wavelengths. The same electron population is believed to produce hard X-rays by inverse-Compton scattering of a photon field. Simultaneous measurements of the polarization angle and the fraction of polarization in the radio to hard X-ray band could help to address the following questions: (i) If the electrons mainly up-scatter the co-spatial synchrotron photon field (synchrotron self Compton), the polarization of the hard X-rays is expected to track the polarization at radio/optical wavelengths.⁹ The fraction of polarization could be a substantial part of the synchrotron fraction of polarization and the polarization directions should be identical. (ii) If the electrons dominantly up-scatter an external photon field (external Compton, e.g. photons of the cosmic microwave background) the hard X-rays will have a relatively small (<10%) fraction of polarization.¹³ Polarization also allows one to test the structure of the magnetic field of the jet: Particles accelerated in a helical field which are moving through a standing shock can cause an X-ray synchrotron flare with a continuous (in time) swing in polarization direction. Such an event was recently observed from BL Lacertae at optical wavelengths¹⁴ and could potentially be observable at X-ray energies, as well.
- *Gamma-ray bursts.* Gamma-ray bursts are believed to be connected to hyper-nova explosions and the formation/launch of relativistic jets.¹⁵ As in the case of the jets in AGN, the structure and particle distribution responsible for gamma-ray bursts will be revealed by X-ray polarization measurements. The X-ray emission of a gamma-ray burst usually lasts for only a few minutes, so that rapid follow-up observations in the X-ray band would be the main challenge.
- *Lorentz invariance.* Hard X-ray polarimetric observations can be used to test/constrain some theories violating Lorentz invariance¹⁶ with unprecedented accuracies by probing the helicity dependence of the speed of light.

For more details on the scientific prospects see for example^{1,17} and references therein. Addressing these science goals requires spectro-polarimetric observations over the broadest possible energy range.

Definitions. If we assume a 100% linearly polarized photon beam, then the minimum/maximum number of counts C_{\min}/C_{\max} of the azimuthal Compton-scattering distribution (histogram) can be used to define the modulation factor: $\mu = (C_{\max} - C_{\min})/(C_{\max} + C_{\min})$. It represents the modulation amplitude of a 100% polarized beam and depends on the polarimeter design and the physics of Compton-scattering. The performance

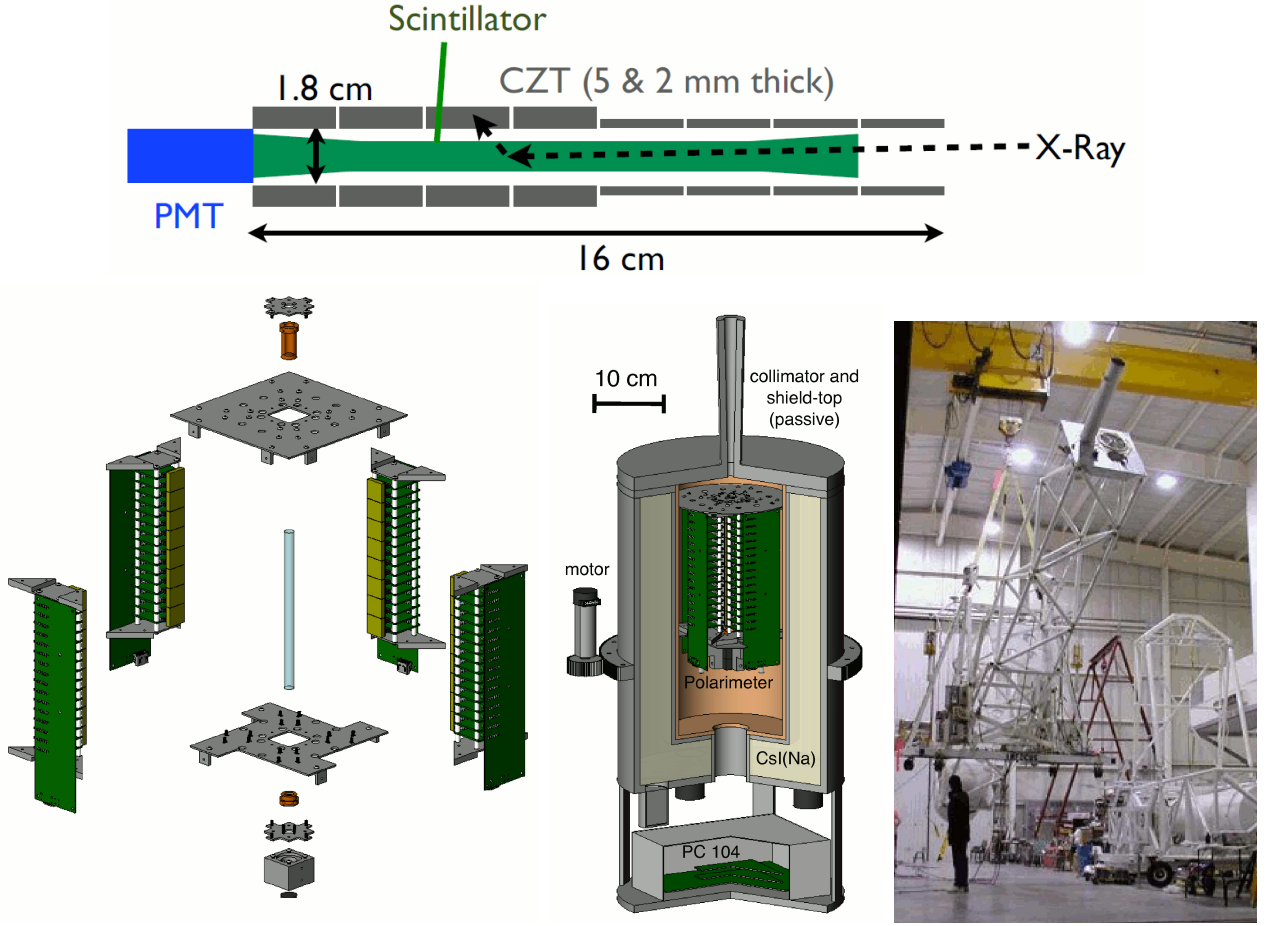


Figure 2. **Top:** Conceptual design of X-Calibur: Incoming X-rays are Compton-scattered in the scintillator rod (read by a PMT) and are subsequently photo-absorbed in a CZT detector. **Lower left:** View of the X-Calibur polarimeter (“exploded view”): 4 sides of CZT detector columns surround the central scintillator rod (optical axis). **Lower middle:** X-Calibur with shielding and azimuthal rotation bearing. **Lower right:** InFOC μ S balloon gondola. X-Calibur will be situated in the focal plane – roughly 8 m away from the Wolter X-ray mirror (40 cm diameter).

of a polarimeter can be characterized by the minimum detectable polarization (MDP) as the minimum fraction of polarization that can be detected at the 99% confidence level. Assuming a polarimeter that detects all Compton-scattered photons and has an ideal angular resolution – in this case μ becomes the modulation amplitude averaged over all solid angles and the Klein-Nishina cross section – one can estimate the MDP by integrating the scattering probability distribution:¹⁸

$$\text{MDP} \simeq \frac{4}{\mu R_{\text{src}}} \sqrt{\frac{R_{\text{src}} + R_{\text{bg}}}{T}} \quad (1)$$

T is the observation time, R_{src} and R_{bg} are the source and background count rates, respectively.

2. DESIGN OF X-CALIBUR

The conceptual design of the X-Calibur polarimeter is illustrated in the top panel of Figure 2. A low-Z scintillator is used as Compton-scatterer for which the cross-section of the photo-effect can be neglected as compared to the cross-section of Compton-scattering for energies > 15 keV (defining the low-energy threshold of X-Calibur).

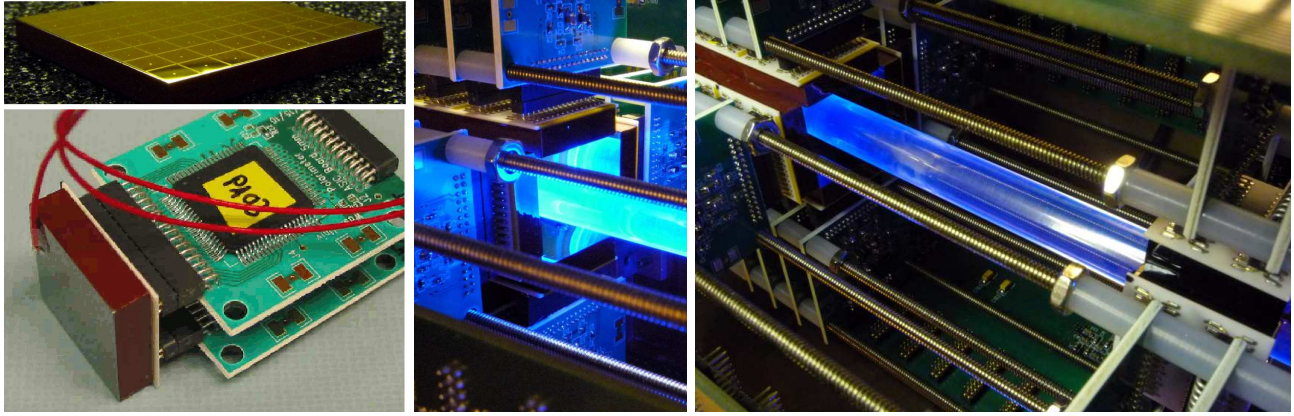


Figure 3. **Left:** Top: $2 \times 2 \times 0.2 \text{ cm}^3$ CZT detector with 64 pixels (anode). Bottom: $2 \times 2 \times 0.5 \text{ cm}^3$ CZT detector bonded to a ceramic chip carrier which is plugged into 2 ASIC readout boards. The high-voltage cable is glued to the detector cathode (red wire). **Middle:** The scintillator (blueish glow) being surrounded by two detector rings – each consisting of four 64 pixel CZT detectors. **Right:** X-Calibur equipped with three detector rings (2 on the left and one on the right).

The length of the scintillator rod is chosen such that even 80 keV photons Compton-scatter with a probability of 90%. For sufficiently energetic photons, the Compton interaction produces a measurable scintillator signal which is read by a PMT. The scattered X-rays are photo-absorbed in surrounding rings of high-Z Cadmium Zinc Telluride (CZT) detectors. This combination of scatterer/absorber leads to a high fraction of unambiguously detected Compton events. Linearly polarized X-rays will preferably Compton-scatter perpendicular to their E field vector – resulting in a modulation of the azimuthal event distribution (see Sec. 1).

The CZT detectors were ordered from different companies (Endicott Interconnect, Quikpak/Redlen, Creative Electron). Each detector ($2 \times 2 \text{ cm}^2$) is contacted with a 64-pixel anode grid (2.5 mm pixel pitch) and a monolithic cathode facing the scintillator rod. Two detector thicknesses (0.2 cm and 0.5 cm) are being tested in the current setup. Each CZT detector is permanently bonded (anode side) to a ceramic chip carrier which can be plugged into the electronic readout board. Figure 3 (left) shows a single CZT detector unit with a 8×8 pixel matrix on the anode side as well as the readout electronics. Each CZT detector is read out by two digitizer boards (32 channel ASIC developed by G. De Geronimo (BNL) and E. Wulf (NRL)¹⁹ and a 12-bit ADC). The readout noise is as low as 2.5 keV FWHM. 16 digitizer boards (8 CZT detectors) are read out by one harvester board transmitting the data to a PC-104 computer with a rate of 6.25 Mbits/s. X-Calibur will comprise 2048 data channels. Four detector units form a 'ring' surrounding the scintillator slab. The scintillator EJ-200 (H:C = 5.17 : 4.69, $\langle Z \rangle = 3.4$, $\rho = 1.023 \text{ g/cm}^3$, decay time 2.1 nsec) is read by a Hamamatsu R7600U-200 PMT with a high quantum efficiency super-bi-alkali photo cathode. The PMT trigger information allows to effectively select scintillator/CZT events from the data which represent likely Compton-scattering candidates. The polarimeter and the front-end readout electronics will be located inside an active CsI(Na) anti-coincidence shield with 5 cm thickness and a passive lead shield/collimator at the top (Fig. 2) to suppress charged and neutral particle backgrounds.

We plan to use the X-Calibur polarimeter in the focal plane of the InFOC μ S* experiment²⁰ (Fig. 2, right). The total mass of the gondola and the X-ray telescope will be 1,400 kg. A Wolter grazing incidence mirror[†] focuses the X-rays on the polarimeter. The X-Calibur scintillator rod will be aligned parallel to the optical axis of the InFOC μ S X-ray telescope. The focal length is $\sim 8 \text{ m}$ and the field of view (FWHM) is $10 \text{ arcmin}^\ddagger$. The design of InFOC μ S allows for very stable pointing of the telescopes to $< 1 \text{ arcmin}$ as the focus of the X-ray telescope moves across the sky. In order to reduce the systematic uncertainties of the polarization measurements (including biases generated by the active shield, a possible pitch of the polarimeter with respect to the X-ray

*<http://infocus.gsfc.nasa.gov/>

[†]Grazing incidence mirrors change the polarization of the X-ray photons by less than 1%²¹

[‡]Note, that the X-Calibur polarimeter does not provide imaging capabilities.

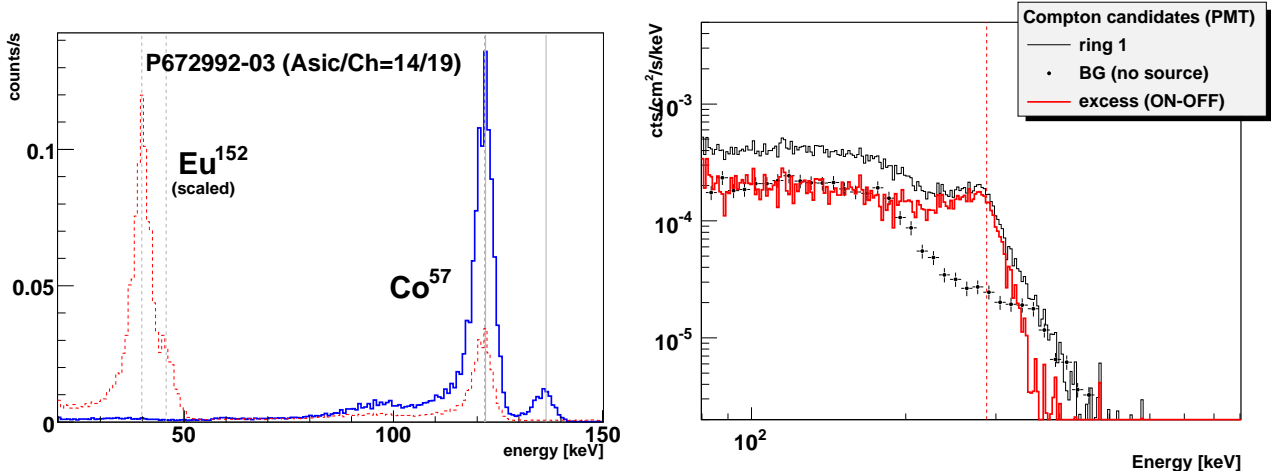


Figure 4. **Left:** Energy spectra of a Eu^{152} source (dashed, scaled) and a Co^{57} source (solid) measured with one pixel of a calibrated CZT detector. The vertical lines indicate the nominal X-ray line energies (from left to right: 39.9 keV, 45.7 keV, 122.1 keV and 136.5 keV). **Right:** Energy spectrum of 288 keV X-rays (partially polarized) after being scattered in the scintillator (different scattering angles and corresponding energy transfer). The background measurement is done without a source (cosmic rays). The vertical line (288 keV) indicates the energy of the incoming X-ray beam.

telescope, etc.), the polarimeter and the active shield will be rotated around the optical axis (~ 10 rpm) using a ring bearing (see Fig. 2, middle). Counter-rotating masses will be used to cancel the net-angular momentum of the polarimeter assembly during the flight. Power will be provided to the polarimeter by sliding contacts and communication will be done via a wireless network. The data will be stored to solid state drives and will be down-linked to the ground. The advantages of the X-Calibur/InFOC μ S design are (i) a high detection efficiency by using more than 80% of photons impinging on the polarimeter, (ii) low background due to the usage of a focusing optics instead of large detector volumes, and (iii) minimization and control of systematic effects and achievement of a corresponding quantitative estimate thereof.

3. SIMULATIONS

Simulations of the X-Calibur polarimeter were performed using the *Geant4* package[§] with the Livermore low-energy electromagnetic model list. All relevant/important effects are included in the simulation starting from the detailed experimental design (see Sec. 2 and Fig. 2), the shielding, the X-ray telescope, as well as several backgrounds. A balloon flight in the focal plane of the InFOC μ S mirror assembly was assumed. The effective detection areas of the X-ray mirror are 95/60/40 cm² at 20/30/40 keV. We accounted for atmospheric absorption at a floating altitude of 130,000 feet using the NIST XCOM attenuation coefficients[¶] and an atmospheric depth of 2.9 g/cm² (observations performed at zenith) – the atmospheric transmissivity rapidly increases from 0 to 0.6 in the 20 – 60 keV range. We simulated the most important backgrounds such as the cosmic X-ray background,²² albedo photons and cosmic ray protons and electrons.²³ The neutron background was not modeled since a detailed study of Parsons et al. (2004) showed that the background contribution in CZT crystals can be neglected.²⁴ A Crab-like source was simulated for a 5.6 hr balloon flight. We assumed a power-law energy spectrum, and a continuous change of the fraction of polarization and the polarization angle between the values measured at 5.2 keV with OSO-8² and at $E > 100$ keV with Integral³ by modeling a transition following a Fermi distribution (Fig. 1, right). The simulation data were analyzed in the same way as the experimental data.

For a Crab-like source the simulations predict an event rate of 1.1(3.2) Hz with (without) requiring a triggered scintillator coincidence detected by the PMT. The X-Calibur modulation factor is $\mu = 0.52$ for a 100% polarized beam. The MDP (see 1) in the 10 – 80 keV energy range will be 4% assuming 5.6 hr of on-source observations

[§]<http://geant4.cern.ch/>

[¶]<http://www.nist.gov/pml/data/xcom/index.cfm>

of a Crab-like source combined with a 1.4 hr background observation of an adjacent empty field. The expected background rates are 0.04(1.1) Hz with (without) requiring a scintillator coincidence. Different shield configurations and shield thicknesses were simulated. The configuration shown in Fig. 2 (middle) represents an optimized compromise balancing the background rejection power and the mass/complexity of the shield.

The results of the simulated X-Calibur observations of the Crab Nebula are compared to the assumed model curves in Figure 1, right; the errors were computed in a similar way as described by Weisskopf et al. (2010).²⁵ Simulations performed at different zenith angles θ show that the sources rate scales with $(\cos \theta)^{1.3}$ which is taken into account for simulating astrophysical observations. More detailed simulations are discussed in Guo et al. (2010).²⁶ Krawczynski et al.¹ present MonteCarlo based comparisons between the performance of X-Calibur with the performance of competing hard X-ray polarimeter designs in the 20 – 100 keV energy range. X-Calibur outperforms the alternative designs by a wide margin.

4. FIRST MEASUREMENTS

Using funding from Washington University’s McDonnell Center for the Space Sciences, a flight-ready version of the X-Calibur polarimeter was assembled and tested in the laboratory. First measurements were performed with 3 detector rings installed (0.5 cm thickness), comprising a total of $3 \times 4 = 12$ detectors (768 data channels). Before installation, IV-curves were taken for all pixels of the detectors, followed by a calibration run using a Eu^{152} source (X-ray lines at 39.9, 45.7, 121.8 and 344.3 keV). An example of the calibration spectrum for one particular detector pixel is shown in Fig. 4, left. The energy resolution for this particular detector is 4.1 keV at 40 keV and 5.0 keV at 121.8 keV. After calibration, a collimated Eu^{152} source was placed in front of the entrance window of the polarimeter in order to determine the azimuthal detector acceptance for an unpolarized beam. Only CZT events with a simultaneous (30 μ s) scintillator trigger are used for this and the following analysis; this is a very effective cut for selecting events of photons that Compton-scattered in the scintillator rod and were subsequently absorbed in one of the CZT detectors. Event rates were normalized by the azimuthal angle $\Delta\Phi$ covered by the corresponding pixel. Another data run was taken without any source to determine the background induced by cosmic rays secondaries hitting the detector assembly.

A polarized beam was generated by scattering a strong Cs^{137} source (line at 662 keV) off a lead brick. A lead collimator allowed only X-rays with a scattering angle of ~ 90 deg to enter the polarimeter. The X-ray beam of the scattered photons has a mean energy of 288 keV and was polarized to $\sim 55\%$ (modulation factor of $\mu = 0.4$). Therefore, the expected relative amplitude in the normalized Φ distribution is $0.55 \times 0.4 = 0.22$.

Figure 4 (right) shows the raw spectrum of the first CZT polarimeter ring measured from (i) the polarized beam, (ii) a background spectrum measured without a source and (iii) the excess spectrum corresponding to the energy spectrum of the scattered/polarized beam. As expected, the excess spectrum drops off for energies higher than 288 keV (vertical line) – the energy of the 90 deg-scattered Cs^{137} photons entering the polarimeter. The continuum below this energy is the result of 288 keV photons being Compton-scattered at different depths in the scintillator rod and therefore being reflected to the first CZT ring under different scattering angles and corresponding different Compton energy losses. The little bump in the spectrum around 288 keV may originate from direct CZT hits without a Compton-scattering in the scintillator.

Figure 5 shows the azimuthal scattering distribution of the polarized and unpolarized beam for the three installed CZT detector rings. Only events with a simultaneous scintillator trigger and with a deposited CZT energy between 100 – 330 keV are used (see spectrum in Fig. 4, right). The data of the polarized beam are corrected for the acceptance of the polarimeter (derived from the unpolarized X-ray beam). As expected for a polarized beam, a 180 deg modulation can be seen with a maximum of azimuthal scattering angle perpendicular ($\Phi + 90$ deg) to the plane of the E field vector of the polarized beam (indicated by the gray arrows). A sine function was fit to the Φ -distribution of the polarized beam resulting in a relative amplitude of 0.22. The data are in excellent agreement with expectations.

5. SUMMARY AND CONCLUSION

We designed a hard X-ray polarimeter X-Calibur and studied its projected performance and sensitivity for a 1-day balloon flight with the InFOC μ S X-ray telescope. X-Calibur combines a detection efficiency of close to

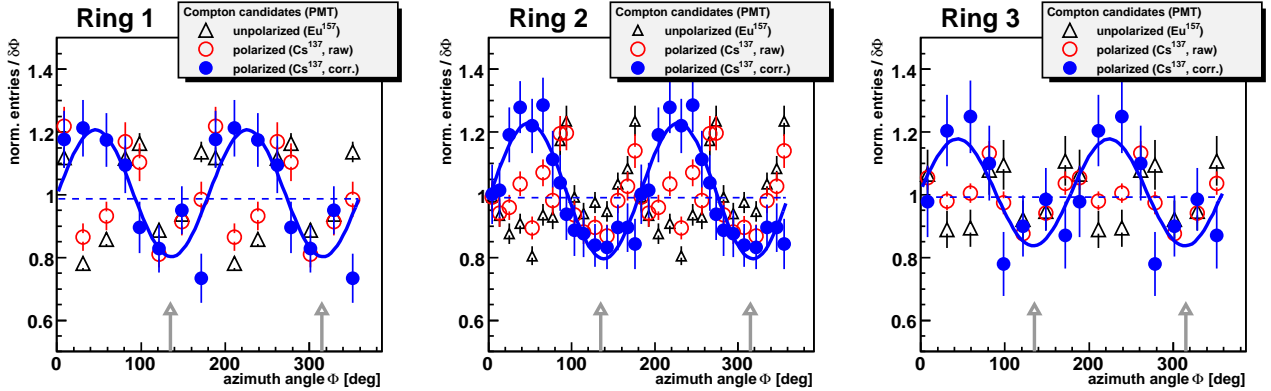


Figure 5. Azimuthal event distribution for the 3 installed CZT detector rings. Shown are raw events of the polarized beam (red), an unpolarized beam (black), and the acceptance corrected polarized events (blue). A sine function (180 deg modulation) was fit to the corrected data of the polarized beam. The vertical arrows indicate the plane of the electric field vector. The 90 deg modulation of the unpolarized beam is a result of the 4-fold geometry of the CZT detector assembly. Ring 1 got less events than ring 2 since it only sees backscatter-events (scintillator starts at ring 2, see Fig. 2), ring 3 got less events since it was not included in the data acquisition at the start of data taking.

100% with a high modulation factor of $\mu \approx 0.5$, as well as a good control over systematic effects. Compared to competing designs of hard X-ray polarimeters X-Calibur does not only have superior sensitivity but also a better energy resolution. X-Calibur was successfully tested/calibrated in the laboratory with a polarized beam of 288 keV photons. Further laboratory measurements are planned to study the effect of different orientations between the polarization plane and the detector, the performance of different CZT detector thicknesses (0.2 cm vs 0.5 cm), the active shielding, and the rotation mechanism.

We applied for a 1-day X-Calibur/InFOC μ S balloon flight in spring 2013. Our tentative observation program includes galactic sources (Crab, Her X-1, Cyg X-1, GRS 1915, EXO 0331) and one extragalactic source (Mrk 421) for which sensitive polarization measurements would be carried through. We envision follow-up longer duration balloon flights (from the northern and southern hemisphere), possibly using a mirror with increased area. An increased mirror area would lead to an increased signal rate while leaving the background rate almost unchanged – resulting in an improved signal-to-noise ratio. In the ideal case these flights would be performed while the GEMS mission is in orbit to achieve simultaneous coverage in the 0.5 – 80 keV regime. Successful balloon flights would motivate a satellite-borne hard X-ray polarimetry mission.

ACKNOWLEDGMENTS

We are grateful for NASA funding from grant NNX10AJ56G and discretionary funding from the McDonnell Center for the Space Sciences to build the X-Calibur polarimeter. Q.Guo thanks the Chinese Scholarship Council from China for the financial support (NO.2009629064) during her stay at Washington University in St. Louis.

REFERENCES

- [1] Krawczynski, H., Garson, A., Guo, Q., Baring, M. G., Ghoshand, P., Beilicke, M., and Lee, K., “Scientific prospects for hard x-ray polarimetry,” *Aph* **34**, 550–567 (2011).
- [2] Weisskopf, M. C., Silver, E. H., Kestenbaum, H. L., Long, K. S., and Novick, R., “A precision measurement of the x-ray polarization of the crab nebula without pulsar contamination,” *ApJ* **220**, L117–L121 (1978).
- [3] Dean, A. J., Clark, D. J., Stephen, J. B., and et al., “Polarized gamma-ray emission from the crab,” *Science* **321**, 1183 (2008).
- [4] Laurent, P., Rodriguez, J., Wilms, J., Bel, M. C., Pottschmidt, K., and Grinberg, V., “Polarized gamma-ray emission from the galactic black hole cygnus x-1,” *Science* **332**, 438 (2011).
- [5] Swank, J. and al., “<http://heasarc.gsfc.nasa.gov/docs/gems/>,” (*online*).

- [6] Tajima, H., Blandford, R., Enoto, T., Fukazawa, Y., Gilmore, K., Kamae, T., Kataoka, J., Kawaharada, M., Kokubun, M., and et al., “Soft gamma-ray detector for the astro-h mission,” *SPIE* **7732**, 34 (2010).
- [7] Schnittman, J. D. and Krolik, J. H., “X-ray polarization from accreting black holes: The thermal state,” *ApJ* **701**, 1175–1187 (2009).
- [8] Korchakov, A. A. and Syrovatskii, S. I., “Polarization of radiation and the structure of magnetic fields in cosmic sources of radiation,” *Soviet Astronomy* **5**, 678 (1962).
- [9] Poutanen, J., “Relativistic jets in blazars: Polarization of radiation,” *ApJS* **92**, 607–609 (1994).
- [10] Connors, P. A. and Stark, R. F., “Observable gravitational effects on polarised radiation coming from near a black hole,” *Nature* **269**, 128 (1977).
- [11] Schnittman, J. D. and Krolik, J. H., “X-ray polarization from accreting black holes: Coronal emission,” *ApJ* **712**, 908–924 (2010).
- [12] Baring, M. G. and Harding, A. K., “Resonant compton upscattering in anomalous x-ray pulsars,” *Astrophysics and Space Science* **308**, 109–118 (2007).
- [13] McNamara, A. L., Kuncic, Z., and Wu, K., “X-ray polarization in relativistic jets,” *MNRAS* **395**, 1507–1514 (2009).
- [14] Marscher, A. P., Jorstad, S. G., D’Arcangelo, F. D., Smith, P. S., Williams, G. G., Larionov, V. M., and et.al., “The inner jet of an active galactic nucleus as revealed by a radio-to-gamma-ray outburst,” *Nature* **452**, 966 (2008).
- [15] Woosley, S. E., “Gamma-ray bursts from stellar mass accretion disks around black holes,” *ApJ* **405**, 273–277 (1993).
- [16] Fan, Y.-Z., Wei, D.-M., and Xu, D., “Gamma-ray burst ultraviolet/optical afterglow polarimetry as a probe of quantum gravity,” *MNRAS* **376**, 1857 (2007).
- [17] Lei, F., Dean, A. J., and Hills, G. L., “Compton polarimetry in gamma-ray astronomy,” *SSRv* **82**, 309 (1997).
- [18] Krawczynski, H., “Analysis of the data from compton x-ray polarimeters which measure the azimuthal and polar scattering angles,” *Aph* **34**, 784–788 (2011).
- [19] Wulf, E. A., Philips, B. F., Johnson, W., and et. al., “Compton imager for detection of special nuclear material,” *NIMA* **579**, 371 (2007).
- [20] Ogasaka, Y., Tueller, J., Yamashita, K., Serlemitsos, P., Shibata, R., and et. al., “First light of a hard-x-ray imaging experiment: the infocus balloon flight,” *SPIE* **5900**, 217–224 (2005).
- [21] Katsuta, J., Mizuno, T., Ogasaka, Y., and et. al., “Evaluation of polarization characteristics of multilayer mirror for hard x-ray observation of astrophysical objects,” *NIMPA* **603**, 393 (2009).
- [22] Ajello, M., Greiner, J., Sato, G., and et al., “Cosmic x-ray background and earth albedo spectra with swift bat,” *ApJ* **689**, 666–677 (2008).
- [23] Mizuno, T., Kamae, T., Godfrey, G., and et al., “Cosmic-ray background flux model based on a gamma-ray large area space telescope balloon flight engineering model,” *ApJ* **614**, 1113–1123 (2004).
- [24] Parsons, A., Barthelmy, S., Bartlett, L., and et al., “Cdznte background measurements at balloon altitudes with portia,” *NIMPA* **516**, 80–95 (2004).
- [25] Weisskopf, M. C., Elsner, R. F., and O’Dell, S. L., “On understanding the figures of merit for detection and measurement of x-ray polarization,” *SPIE* **7732**, 11 (2010).
- [26] Guo, Q., Garson, A., Beilicke, M., Martin, J., Lee, K., and Krawczynski, H., “Design of a hard x-ray polarimeter: X-calibur,” *arXiv* **1101.0595**, 1–5 (2010).